Original

Automatic Prostate Cancer Segmentation Using Kinetic Analysis in Dynamic Contrast-Enhanced MRI

Navaei Lavasani S.[1], Mostaar A.[1,*], Ashtiyani M.[1]

[1]Department of Biomedical Engineering and Medical Physics, Faculty of Medicine, Shahid Beheshti University of Medical Sciences, Tehran, Iran

ABSTRACT

Background: Dynamic contrast enhanced magnetic resonance imaging (DCE-MRI) provides functional information on the microcirculation in tissues by analyzing the enhancement kinetics which can be used as biomarkers for prostate lesions detection and characterization.

Objective: The purpose of this study is to investigate spatiotemporal patterns of tumors by extracting semi-quantitative as well as wavelet-based features, both extracted from pixel-based time-signal intensity curves to segment prostate lesions on prostate DCE-MRI.

Methods: Quantitative dynamic contrast-enhanced MRI data were acquired on 22 patients. Optimal features selected by forward selection are used for the segmentation of prostate lesions by applying fuzzy c-means (FCM) clustering. The images were reviewed by an expert radiologist and manual segmentation performed as the ground truth.

Results: Empirical results indicate that fuzzy c-mean classifier can achieve better results in terms of sensitivity, specificity when semi-quantitative features were considered versus wavelet kinetic features for lesion segmentation (Sensitivity of 87.58% and 75.62%, respectively) and (Specificity of 89.85% and 68.89 %, respectively).

Conclusion: The proposed segmentation algorithm in this work can potentially be implemented for automatic prostate lesion detection in a computer aided diagnosis scheme and combined with morphologic features to increase diagnostic credibility

Introduction

Early detection and evaluation of prostate cancer as the most common cause of cancer death worldwide are issues of major concern [1]. Nowadays, the use of prostate-specific antigen (PSA) serum screening and Digital Rectal Examination (DRE) have increased the diagnosis of prostate cancer. One shortcoming with the current standard of care followed by transrectal ultrasonography (TRUS), guided biopsy, is low sensitivity that leads to random biopsy. In this method, it is possible to miss a large tumor outside usual biopsy template [2, 3]. An important role of noninvasive imaging technique is to help guide biopsies, radiotherapy and surgery as well as to monitor disease pro-

*Corresponding author:
A. Mostaar, PHD
Department of Biomedical Engineering and Medical Physics, Faculty of Medicine, Shahid Beheshti University of Medical Sciences, Tehran, Iran
E-mail: mostaar@sbmu.ac.ir

gression. Many studies have shown the ability of multi-parametric MRI (mpMRI) to demonstrate tumor morphology and the relationships of malignant lesions with neighboring structures and providing essential clinical information on the detection of prostate cancer [4]. Visualization and localization of prostate cancer can be improved by mpMRI which involves the acquisition of T2-weighted (T2W) images, diffusion-weighted images, MR spectroscopy and dynamic contrast-enhanced (DCE) MRI [3, 5-8]. Dynamic contrast enhanced magnetic resonance imaging (DCE-MRI) is a functional modality which involves the administration of a paramagnetic contrast agent (CA), and subsequently, the assessment of T1-weighted MR images of tissue of interest (e.g., a tumor) pre- and post-intravenous injection [9]. Many tumors have distinctive enhancement patterns which may provide useful diagnostic or staging information [10]. Prostate cancer generally results in faster and higher levels of enhancement than normal tissue [11]. The interpretation of prostate DCE-MR images is a challenging task even for an expert radiologist due to the large information included in 4D images. Furthermore, since manual segmentation is too time-consuming, occurrence of human error is highly susceptible. Hence, detection of prostate cancerous tissues using a computerized automated segmentation technique is desirable.

Recently, some innovations of computer-aided algorithms have been successfully applied in prostate mutliparametric MRI images. Artan et al. [12] proposed a supervised learning algorithm to automate prostate cancer localization with conditional random fields using multispectral MRI. Liu et al. [13] presented an unsupervised method for prostate cancer detection, using fuzzy Markov random fields (fuzzy MRFs). Guo et al. [14] showed fuzzy information related to cancerous tissue on each kind of MRI data could precisely extract cancerous regions of the prostate. In this paper, we evaluated the intensity changes of 3D DCE-MRI time courses to segment prostate tumors. In addition, the efficiency of different patterns of perfusion time courses extracted by semi-quantitative and wavelet-based features in segmentation of prostate cancer are also compared. This approach consists of 1) semi-quantitative and discrete wavelets transform analysis of voxel time courses, and 2) fuzzy c-means clustering of the wavelet coefficients and semi-quantitative features to segment prostate tumors. Our method provides an automated approach to prostate tumors segmentation.

Material and Methods

Imaging Protocol

DCE-MR images of 22 patients diagnosed with prostate cancer were acquired on a 3T MR scanner (GE Healthcare, Waukesha, WI) using a combination of 8-channel abdominal array and endorectal coil (Medrad, Pittsburgh, PA). DCE MRI utilized a 3D SPGR sequence with TE/TR = 3.6/1.3 ms, flip angle = 15°, image matrix = 256×256, FOV = 26×26 cm^2, slice thickness = 6 mm, number of measurements = 60 at 5 sec/volume, number of slices = 12 and 16. At first, five baseline dynamic scans were performed before the injection of contrast agent and the subsequent scans started immediately after the injection of 3 mL/sec of Gadolinium, followed by 20 ml saline flush at the same rate. The database was provided by QIN Prostate database of The Cancer Imaging Archive (TCIA)[15].

Motion Correction Algorithm

The monitoring of contrast agent uptake and washout takes minutes. Motion Artifacts due to body movements of the patient or physiologic movements such as breathing are usually inevitable during DCE-MRI data acqui-

sition. Proper registration of dynamic images acquired at different time-points is essential for deriving accurate diagnostic information from quantitative analysis of DCE-MRI data [16]. Before analysis of enhancement curves, all image series were aligned using a three-dimensional (3-D) voxel property-based [17]. The transformation is obtained by optimizing the spatial similarity defined by sum of squared intensity differences (SSD) between the image under investigation and a reference image [18]. The reference dataset was set to average of pre-contrast series; each post-contrast was registered with the reference image. After 3-D registration, the motion artifact was minimized and the time intensity curves (TICs) obtained was accurate.

Manual ROI Segmentation

The morphological images (Turbo spin-echo T2- and T1-weighted) and functional fat-suppressed DCE-MR images were reviewed by an expert radiologist in a slice-by-slice fashion and regions of interest (ROIs) were manually placed within the prostate. For each patient, all slices including the lesions were used in the analysis. The segmentation was performed using ImageJ software [19].

Kinetic Features Extraction
Semi-quantitative Features

Manual segmentation of prostate lesions is both time-consuming and highly susceptible to human error which leads to lack of reproducibility. In this light, devising accurate automated lesion segmentation techniques are highly desirable. Dynamic contrast-enhanced MRI has added an extra temporal dimension to the existing spatial dimensions. The dynamic acquisition for each voxel in DCE-MRI contains sequence of measurements over time. The variation in shape of signal enhancement in each voxel is strongly related to blood flow and physiological properties of tissue. Numer-

ous studies using dynamic contrast enhanced MRI have demonstrated that malignant tumors usually demonstrate more intense enhancement compared to normal tissues [20-24]; the pixels with more enhancements are initially considered as suspected lesions. To segment prostate tumors from 3D DCE-MR image, the signal intensity values of the whole image voxels at consequent time-steps were normalized to the pre-contrast signal intensity [25], and relative enhancement is calculated according to the following equation:

$$RE = \frac{(SIpost - SIpre)}{SIpre} \qquad (1)$$

Where, for each pixel SIpre is the signal intensity in the pre-contrast image, while SIpost is the signal intensity in the post-contrast image [3, 22, 26, 27]. Based on relative enhancement signal intensity-time curves of each pixel, semi-quantitative features were extracted (Figure 1). Commonly used kinetic parameters in DCE-MRI context, namely initial enhancement rate, maximal enhancement rate and amplitude as well as enhancement rate at various time points were calculated for each voxel as indicated in Table 1.

Wavelet Kinetic Features

In DCE-MR images, the pixels related to prostate tumors indicate heterogeneous behavior both spatially and temporally. This kind of intra-tumor heterogeneity poses a major challenge for cancer detection and diagnosis. The discrete wavelet transform (DWT) is an appropriate detection tool to evaluate transient changes in time series, and may provide valuable features from time series in imaging experiments such as DCE-MR images [28]. The multi-resolution properties of the wavelet transform present it as a reasonable candidate to match high-frequency transients and slowly varying harmonics characteristics of signal. As a second approach to segment prostate tumors from 3D DCE-MR image, we applied wavelet
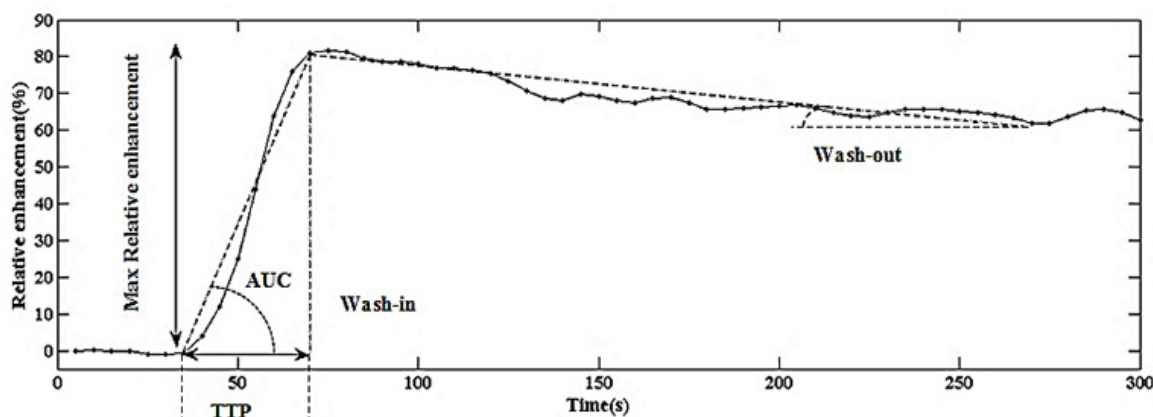
Figure 1: Relative time intensity curve. The different parameters that were calculated (Max Relative enhancement, TTP, Wash-in, Wash-out and Area under curve (AUC)) are illustrated on a pixel of malignant prostatic tissue.

analysis to the pixel-based time-signal intensity curves, and heterogeneity wavelet kinetic features were extracted to obtain spatiotemporal patterns of contrast agent from pixels [29].

Basically, wavelet transform is a mathematical function which decomposes data into different scales and defines a sparse representation of data. The DWT of a signal uses a different time window for each scale translating window across the signal, and compares the wavelet to that of the signal to derive a correlation coefficient [30].

Two level decompositions of Haar wavelet family were calculated in wavelet transformation of the signal intensity-time curves of the whole pixels of prostate images [31]. In addition, mean and variance of the approximation and detail coefficients of each level were extracted. Our final feature vector thus consisted of 6 features for each TIC.

FCM Clustering

The fuzzy c-mean (FCM) clustering algorithm was first introduced by Dunn and later extended by Bezdek [32]. This algorithm is an iterative clustering method and presents some

Table 1: Description of semi-quantitative parameters

Parameter	Description
SImax	Maximum relative enhancement
IAUC60	Initial area under the time-intensity curve during the first 60 seconds of the bolus passage
TTP	Time-to-Peak: the time to the maximum absolute enhancement
WIR	Wash-in-Rate
WOR	Wash-out-rate
SER	Signal enhancement ratio $= \dfrac{RE_1 - RE_0}{RE_g - RE_0}$

advantages with respect to other classifiers, being one of the most important high generalization capacity for a reduced number of training trials [33, 34]. FCM is an extensively used technique that uses the principles of fuzzy sets to evolve a partition matrix while minimizing the measure:

$$J(M,C) = \sum_{n=1}^{N}\sum_{k=1}^{K} m_{nk}^{f} D(p_n, c_k) \qquad (2)$$

Where N is the number of data objects, K represents number of clusters, M is the fuzzy membership matrix (partition matrix) and f ($f > 1$) denotes the fuzzy exponent that controls the amount of fuzziness. Here p_n is the nth data point and c_k is the center of the kth cluster [35]. $D(p_n, c_k)$ denotes the distance of point p_n from the center of the kth cluster. Generally, the Euclidean distance measure has been used as a measure of the distance between two points [34, 36].

The FCM technique is applied in this study on DCE-MRI data. For semi-quantitative and wavelet-based features, optimal features were selected by forward selection [37].

Evaluation

An objective method is needed to evaluate the performance of the new proposed image segmentation algorithm. The radiologist manually specified all tumors, and the manual segmentation results were used as the reference to evaluate the algorithm. The performance of the proposed algorithm was verified in terms of sensitivity, specificity, accuracy, Jaccard index and Dice score measures, against manual segmentation performed by an expert radiologist as the ground truth.

If I_1 and I_2 are automated and manual segmentations of an image, respectively, then $T_p = I_1 \cap I_2$ will be the true positive, and $F_p = I_1 - I_2$, $F_n = I_2 - I_1$ will be the false positive and false negative, respectively [38]. Sen-

sitivity and specificity are defined as:

$$\text{Sensitivity} = \frac{T_p}{T_p + F_n} \qquad (3)$$

$$\text{Specificity} = \frac{T_n}{T_n + F_p} \qquad (4)$$

Accuracy is defined as:

$$\text{Accuracy} = \frac{T_p + T_n}{T_p + T_n + F_p + F_n} \qquad (5)$$

The Dice similarity coefficient represents spatial overlap and reproducibility [39]. Similarity is defined as:

$$Dice(I_1, I_2) = \frac{2|I_1 \cap I_2|}{|I_1| + |I_2|} \qquad (6)$$

and Jaccard index is defined as:

$$J(I_1, I_2) = \frac{2|I_1 \cap I_2|}{I_1 \cup I_2} \qquad (7)$$

Results

Figure 2 shows three examples of the segmentation results and illustrates the comparison between manual and two automated segmentation methods. In the first method, the lesions are segmented by kinetic features including REmax, AUC60 and WOR selected by forward selection Figure 2 (b, e, h), and in the second approach, they are delineated by wavelet kinetic features selected by forward selection containing variance of approximation and detail components in two levels of decomposition as apparent from Figure 2 (c, f, i). As it is evident from these figures, the segmentation performed based upon semi-quantitative parameters is very close to the manual segmentation. In particular, it can be observed from Figure 2 that the segmentation by semi-quantitative features (Figure 1 (b,
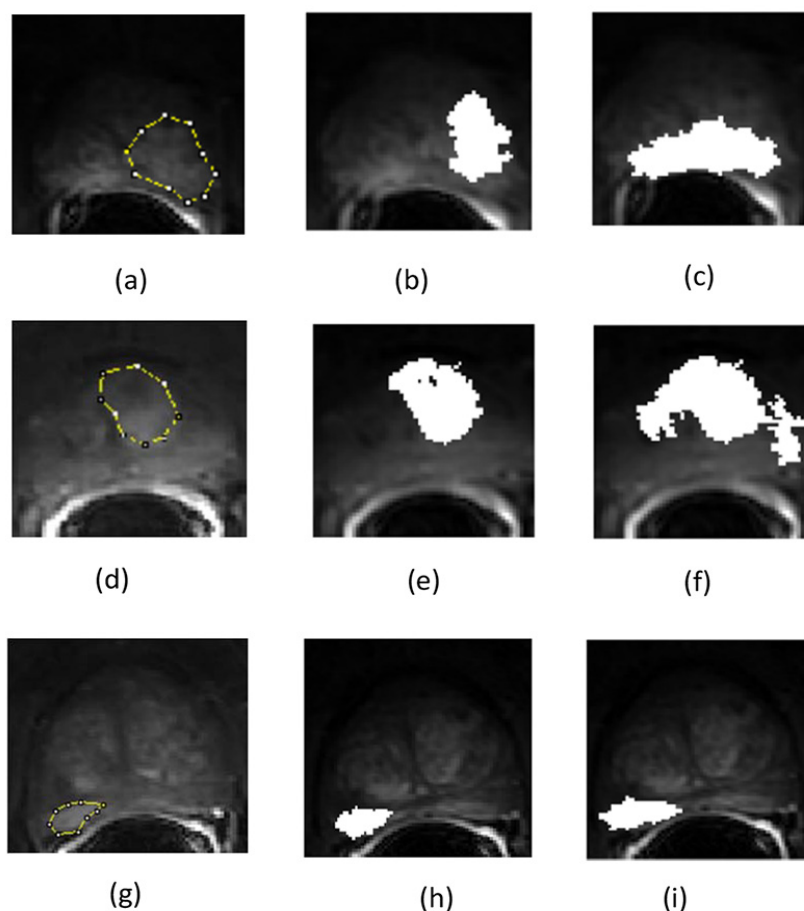
Figure 2: Segmentation of DCE-MRI images (Patient 1, 2, 3). (a, d, g) Tumor outlined by a pathologist, (b, e, h) The segmentation result by the Semi-quantitative features, (d, f, i) and by the Wavelet based features.

e, h)) is more robust to noisy pixels than the second method. Average of sensitivity, specificity, accuracy, Dice score and Jaccard index were calculated across all lesions, for each of the two automatic segmentation methods. In Table 2, evaluation results of the two methods of segmentation are summarized, the performance of the technique based on semi-quan-

titative features outperformed wavelet kinetic features.

Discussion

In this study, we presented a new pixel-wise automatic segmentation method which works based on kinetic features derived from wavelet transformation of signal intensity curves and

Table 2: Evaluation the performance of two methods of segmentation

	Accuracy	Sensitivity	Specificity	Dice	Jaccard
Semi-quantitative	80.23%	87.58%	89.85%	83.82%	72.28%
Wavelet-kinetic	71.43%	75.62%	68.89%	78.43%	69.32%

semi-quantitative parameters in high temporal-resolution 3D DCE-MR images. Thereby, we take advantages of the signal intensities evolving over time which exhibit characteristic patterns related to the cancerous regions of the prostate [26]. This allows for a discrimination of prostate tumors from benign peripheral zone as demonstrated by our study.

Manual selection of ROI in DCE-MRI, due to the heterogeneity of tumor and large volume of 3D data, is problematic and operator dependent. An automatic method for DCE-MRI data analysis may be of value to assist detection of prostate tumor in MRI. To segment prostate cancer from 3D DCE-MR image, we applied a semi-quantitative and wavelet analysis to the time series of each voxel and used FCM to cluster the features to partition different parts of the prostate. Results from the automated pixel-by-pixel segmentation indicate a statistically significant difference in semi-quantitative parameters between tumor and normal prostatic tissue. There was no significant difference in the wavelet kinetic parameters between cancerous and normal tissues. Semi-quantitative analysis has a wide application in the diagnosis and detection of tumors in DCE-MRI [3, 11, 40]. Jackson et al. [41] proposed a pixel by pixel quantitative analysis to investigate the accuracy of DCE-MRI for prostate cancer detection. Prostate tumor was detected by pharmacokinetic parameter and detection results were compared with histology, and the accuracy of DCE-MRI and T2W images in tumor detection was then evaluated. Results approved pharmacokinetic parameters have relative discrimination between cancer and benign gland and DCE-MRI demonstrates more sensitivity and specificity than T2W images in prostate cancer detection. Isebaert et al. [26] evaluated the efficiency of semi-quantitative parameters in prostate cancer detection in correlation to whole-mount histopathology. Regions of interest (ROIs) and

normal prostatic tissue on DCE images were manually selected. Results showed distinct differences between Wash-in parameter, alone or in combination with the Wash-out of malignant versus benign tissue. In previous studies, some automatic prostate segmentation methods were proposed. Artan et al. [2] developed methods based on the combination of cost-sensitive Support Vector Machines with Conditional Random Fields to automated detection of prostate cancer. Based on results, the proposed method has high accuracy in prostate cancer localization in multispectral MRI. Guo et al. [14] presented automatic prostate cancer segmentation method based on multiparametric MRI features by implying FCM clustering. Presented method by extracting parameter maps contains T2w MRI image intensity (Cit/($Cho+Cr$), ADC, k_{ep}) localized prostate cancer in both peripheral zone and transition zones.

In this paper, we presented an automatic scheme based on Fuzzy c-mean clustering (FCM) using semi-quantitative and wavelet-kinetic features extracted from signal intensity-time curves and for prostate tumors segmentation in DCE-MR images. Results showed distinct differences between extracted kinetic features of malignant versus benign tissues. Based on the variations in prostate tumors shape, this paper suggests that the proposed parameters can be used as potential indicators for the prostate tumor detection and localization. Our segmentation method manifested an acceptable performance in segmentation of prostate DCE-MRI with accuracy of 80.23%, sensitivity of 87.58% and specificity of 89.85% for semi-quantitative features.

Conclusion

In this study, we proposed a new pixel-wise automatic segmentation method that works based on kinetic features derived from wavelet transformation of signal intensity curves and semi-quantitative parameters. From our ex-

periments, we conclude that semi-quantitative based FCM clustering is a feasible approach to segment prostate tumors in DCE-MRI. Initial findings based on semi-quantitative features show promising results with higher segmentation accuracy than wavelet kinetic features compared to manual delineations, which could accurately and reliably discriminate tumorous lesions from other parts in high temporal-resolution DCE-MR images.

Conflict of Interest

None

References

1. Stamey TA, Caldwell M, McNeal JE, Nolley R, Hemenez M, Downs J. The prostate specific antigen era in the United States is over for prostate cancer: what happened in the last 20 years? *J Urol*. 2004;**172**:1297-301. doi.org/10.1097/01.ju.0000139993.51181.5d. PubMed PMID: 15371827.

2. Artan Y, Langer DL, Haider MA, van der Kwast TH, Evans AJ, Wernick MN, et al. Prostate cancer segmentation with multispectral MRI using cost-sensitive conditional random fields. 28 June-1 July 2009 . Boston: Biomedical Imaging: From Nano to Macro, 2009 ISBI'09 IEEE International Symposium on; 2009.

3. Verma S, Turkbey B, Muradyan N, Rajesh A, Cornud F, Haider MA, et al. Overview of dynamic contrast-enhanced MRI in prostate cancer diagnosis and management. *AJR Am J Roentgenol*. 2012;**198**:1277-88. doi.org/10.2214/AJR.12.8510. PubMed PMID: 22623539.

4. Mostaar A, Ashtiyani M, Lavasany SN, Rexhepi AH, Kongoli R, Dey A, et al. AAn Improved Ant Colony Algorithm Optimization for Automated MRI Segmentation Using Probabilistic Atlas. Int J Innov Res Sci Eng. 2015;3:399, 406.

5. Turkbey B, Bernardo M, Merino MJ, Wood BJ, Pinto PA, Choyke PL. MRI of localized prostate cancer: coming of age in the PSA era. *Diagn Interv Radiol*. 2012;**18**:34-45. PubMed PMID: 21922459.

6. Puech P, Betrouni N, Makni N, Dewalle AS, Villers A, Lemaitre L. Computer-assisted diagnosis of prostate cancer using DCE-MRI data: design, implementation and preliminary results. *Int J Comput Assist Radiol Surg*. 2009;**4**:1-10. doi.org/10.1007/

s11548-008-0261-2. PubMed PMID: 20033597.

7. van Dorsten FA, van der Graaf M, Engelbrecht MR, van Leenders GJ, Verhofstad A, Rijpkema M, et al. Combined quantitative dynamic contrast-enhanced MR imaging and 1H MR spectroscopic imaging of human prostate cancer. *Journal of Magnetic Resonance Imaging*. 2004;**20**:279-87. doi.org/10.1002/jmri.20113.

8. Futterer JJ, Heijmink SW, Scheenen TW, Veltman J, Huisman HJ, Vos P, et al. Prostate cancer localization with dynamic contrast-enhanced MR imaging and proton MR spectroscopic imaging 1. *Radiology*. 2006;**241**:449-58. doi.org/10.1148/radiol.2412051866.

9. Yankeelov TE, Gore JC. Dynamic Contrast Enhanced Magnetic Resonance Imaging in Oncology: Theory, Data Acquisition, Analysis, and Examples. *Curr Med Imaging Rev*. 2009;**3**:91-107. doi.org/10.2174/157340507780619179. PubMed PMID: 19829742. PubMed PMCID: 2760951.

10. Birgani PM, Ashtiyani M, editors. Wireless Real-time Brain Mapping. 27-30 Nov. 2006. Guilin: Communication Technology, 2006 ICCT'06 International Conference on; 206.

11. Engelbrecht MR, Huisman HJ, Laheij RJ, Jager GJ, van Leenders GJ, Hulsbergen-Van De Kaa CA, et al. Discrimination of prostate cancer from normal peripheral zone and central gland tissue by using dynamic contrast-enhanced MR imaging. *Radiology*. 2003;**229**:248-54. doi.org/10.1148/radiol.2291020200. PubMed PMID: 12944607.

12. Artan Y, Haider MA, Langer DL, van der Kwast TH, Evans AJ, Yang Y, et al. Prostate cancer localization with multispectral MRI using cost-sensitive support vector machines and conditional random fields. *IEEE Trans Image Process*. 2010;**19**:2444-55. doi.org/10.1109/TIP.2010.2048612. PubMed PMID: 20716496.

13. Liu X, Langer DL, Haider MA, Yang Y, Wernick MN, Yetik IS. Prostate cancer segmentation with simultaneous estimation of Markov random field parameters and class. *IEEE Trans Med Imaging*. 2009;**28**:906-15. doi.org/10.1109/TMI.2009.2012888. PubMed PMID: 19164079.

14. Guo Y, Ruan S, Walker P, Feng Y, editors . Prostate cancer segmentation from multiparametric MRI based on fuzzy Bayesian model. 29 April-2 May 2014. Beijing: Biomedical Imaging (ISBI), 2014 IEEE 11th International Symposium on; 2014.

15. Clark K, Vendt B, Smith K, Freymann J, Kirby J, Koppel P, et al. The Cancer Imaging Archive (TCIA):

maintaining and operating a public information repository. *J Digit Imaging*. 2013;**26**:1045-57. doi.org/10.1007/s10278-013-9622-7. PubMed PMID: 23884657. PubMed PMCID: 3824915.

16. Lu W, Yao J, Lu C, Prindiville S, Chow C, editors. DCE-MRI segmentation and motion correction based on active contour model and forward mapping. 19-20 June 2006. Las Vegas: Software Engineering, Artificial Intelligence, Networking, and Parallel/Distributed Computing, 2006 SNPD 2006 Seventh ACIS International Conference on; 2006.

17. Maintz JA, Viergever MA. A survey of medical image registration. *Medical image analysis*. 1998;**2**:1-36. doi.org/10.1016/S1361-8415(01)80026-8.

18. Chen CJ, Chang RF, Moon WK, Chen DR, Wu HK. 2-D ultrasound strain images for breast cancer diagnosis using nonrigid subregion registration. *Ultrasound Med Biol*. 2006;**32**:837-46. doi.org/10.1016/j.ultrasmedbio.2006.02.1406. PubMed PMID: 16785006.

19. Schneider CA, Rasband WS, Eliceiri KW. NIH Image to ImageJ: 25 years of image analysis. *Nat Methods*. 2012;**9**:671-5. doi.org/10.1038/nmeth.2089. PubMed PMID: 22930834.

20. Padhani AR. Dynamic contrast-enhanced MRI studies in human tumours. *Br J Radiol*. 1999;**72**:427-31. doi.org/10.1259/bjr.72.857.10505003. PubMed PMID: 10505003.

21. Alonzi R, Padhani AR, Allen C. Dynamic contrast enhanced MRI in prostate cancer. *Eur J Radiol*. 2007;63:335-50. doi.org/10.1016/j.ejrad.2007.06.028. PubMed PMID: 17689907.

22. Navaei-Lavasani S, Fathi-Kazerooni A, Saligheh-Rad H, Gity M. Discrimination of Benign and Malignant Suspicious Breast Tumors Based on Semi-Quantitative DCE-MRI Parameters Employing Support Vector Machine. *Frontiers in Biomedical Technologies*. 2015;**2**:87-92.

23. Fotouhi A, Eqlimi E, Makkiabadi B, editors. Evaluation of adaptive parafac alogorithms for tracking of simulated moving brain sources. 25-29 Aug. 2015. Milan: Engineering in Medicine and Biology Society (EMBC), 2015 37th Annual International Conference of the IEEE; 2015.

24. Eqlimi E. Resting State Functional Connectivity Analysis Based on Mutual Information Graphs For MS Patients. 2013.

25. Kuhl CK, Mielcareck P, Klaschik S, Leutner C, Wardelmann E, Gieseke J, et al. Dynamic breast MR imaging: are signal intensity time course data useful for differential diagnosis of enhancing lesions? *Radiology*. 1999;**211**:101-10. doi.org/10.1148/radiology.211.1.r99ap38101. PubMed PMID: 10189459.

26. Isebaert S, De Keyzer F, Haustermans K, Lerut E, Roskams T, Roebben I, et al. Evaluation of semi-quantitative dynamic contrast-enhanced MRI parameters for prostate cancer in correlation to whole-mount histopathology. *Eur J Radiol*. 2012;**81**:e217-22. doi.org/10.1016/j.ejrad.2011.01.107. PubMed PMID: 21349667.

27. Navaei Lavasani S, Fathi Kazerooni A, Saligheh Rad H, Gity M. Discrimination of Benign and Malignant Suspicious Breast Tumors Based on Semi-Quantitative DCE-MRI Parameters Employing Support Vector Machine. *Frontiers in Biomedical Technologies*. 2015;**2**:87-92.

28. Unser M, Aldroubi A. A review of wavelets in biomedical applications. *Proceedings of the IEEE*. 1996;**84**:626-38. doi.org/10.1109/5.488704.

29. Mallat S. A wavelet tour of signal processing: Academic press. Cambridge: Academic press; 1999.

30. Poularikas AD. Transforms and applications handbook. Florida: CRC press; 2010.

31. Struzik ZR, Siebes A, editors. The Haar wavelet transform in the time series similarity paradigm. European Conference on Principles of Data Mining and Knowledge Discovery: Springer; 1999.

32. Birgani PM, Ashtiyani M, Asadi S, editors. MRI segmentation using fuzzy c-means clustering algorithm basis neural network. 7-11 April 2008. Damascus: Information and Communication Technologies: From Theory to Applications, 2008. ICTTA 2008. 3rd International Conference on; 2008.

33. Ashtiyani M, Asadi S, Birgani PM, editors . ICA-based EEG classification using fuzzy c-mean algorithm. 7-11 April 2008. Damascus. Information and Communication Technologies: From Theory to Applications, 2008 ICTTA 2008 3rd International Conference on; 2008.

34. Ashtiyani M, Behbahani S, Asadi S, Birgani PM, editors . Transmitting encrypted data by wavelet transform and neural network. 15-18 Dec. 2007. Giza: Signal Processing and Information Technology, 2007 IEEE International Symposium on; 2007.

35. Mansoory MS, Ashtiyani M, Sarabadani H. Automatic crack detection in eggshell based on SUSAN Edge Detector using Fuzzy Thresholding. *Modern Applied Science*. 2011;**5**:117. doi.org/10.5539/mas.v5n6p117.

36. Bezdek JC, Ehrlich R, Full W. FCM: The fuzzy c-

means clustering algorithm. *Computers & Geosciences*. 1984;**10**:191-203. doi.org/10.1016/0098-3004(84)90020-7.

37. Kohavi R, John GH. Wrappers for feature subset selection. *Artificial intelligence*. 1997;**97**:273-324. doi.org/10.1016/S0004-3702(97)00043-X.

38. Jamshidi O, Pilevar AH. Automatic segmentation of medical images using fuzzy c-means and the genetic algorithm. *Journal of Computational Medicine*. 2013;2013.

39. Udupa JK, Leblanc VR, Zhuge Y, Imielinska C, Schmidt H, Currie LM, et al. A framework for evaluating image segmentation algorithms. *Comput Med Imaging Graph*. 2006;**30**:75-87. doi.org/10.1016/j.compmedimag.2005.12.001. PubMed PMID: 16584976.

40. Medved M, Karczmar G, Yang C, Dignam J, Gajewski TF, Kindler H, et al. Semiquantitative analysis of dynamic contrast enhanced MRI in cancer patients: Variability and changes in tumor tissue over time. *J Magn Reson Imaging*. 2004;**20**:122-8. doi.org/10.1002/jmri.20061. PubMed PMID: 15221817.

41. Jackson A, Reinsberg S, Sohaib S, Charles-Edwards E, Jhavar S, Christmas T, et al. Dynamic contrast-enhanced MRI for prostate cancer localization. *The British journal of radiology*. 2014.